Cite this: *Soft Matter*, 2012, **8**, 11328

www.rsc.org/softmatter

PAPER

Diblock copolymer–selective nanoparticle mixtures in the lamellar phase confined between two parallel walls: a mean field model

Lenin S. Shagolsem*[ab] and Jens-Uwe Sommer[ab]

Received 2nd July 2012, Accepted 26th August 2012
DOI: 10.1039/c2sm26531a

We present a mean field model for a mixture of AB diblock-copolymers and A-block selective nanoparticles confined between two identical non-selective walls. A horizontally symmetric lamellar structure of the nanocomposite is considered where nanoparticles are allowed to segregate between the polymer–wall interfaces. For a fixed value of wall separation, we study changes in the free energy as a function of the number of lamellar layers and the amount of nanoparticle uptake in the A-phase denoted by $y = \phi x$ with $0 \leq x \leq 1$ for a given value of ϕ, where ϕ is the overall nanoparticle volume fraction. The absorption isotherm for nanoparticle uptake in the A-phase as a function of ϕ shows saturation beyond a threshold value ϕ_s, and the optimal value of uptake y increases with increasing strength of monomer–nanoparticle attractive interaction. Increasing ϕ above ϕ_s produces a decrease in the optimal number of lamellar layers which is related to a jump-like transition of the chain extension. The effect of varying film thickness is also studied. By considering A-block selective walls we also investigated a wetting transition of the copolymer film and found the transition to be discontinuous. A corresponding phase diagram is constructed.

I. Introduction

Diblock-Copolymers (DBCs), created by covalently joining two chemically distinct polymer blocks, are very suitable for producing flexible nanocomposite materials that exhibit advantageous electrical, optical, and mechanical properties. For example, DBC and nanoparticle (NP) mixtures are used in the creation of next generation catalysts, selective membranes, photonic band gap materials and stimuli-responsive materials.[1–4] Block-copolymers which microphase separate into various nanostructures[5] can direct the spatial distribution of NPs in the polymer matrix. Generally, two types of NPs are distinguished with respect to their monomer affinity: selective NPs which prefer one component of DBC, and nonselective NPs which interact equally with both components of DBC.[6]

Block-copolymers in geometrical constraints (thin-films) are of particular interest since many applications are based on thin-film technologies. For thin-films, confining geometries as well as the interaction of the copolymer components and NPs with respect to the confining surfaces have to be considered and this leads to a many-dimensional phase diagram and corresponding parameter space which may be used to tune the order and morphology of the nanocomposite films. A basic understanding of the interplay of the various parameters by considering simplified models for the DBC–NP composite is necessary for both a rational design of new composite film materials and more rigorous numerical and theoretical investigations of the most promising combinations of parameters.

Recent studies on DBC–NP mixtures show that NPs can induce self-assembled structures.[7–11] Segregation of nonselective NPs at the DBC interface and at the polymer–wall interface for confined systems is observed.[11–18] The driving force behind the migration of non-selective NPs at the interfaces in the nonselective case can be the entropic depletion effect which arises due to the size difference between monomers and NPs.[15,16,19] Selective NPs, on the other hand, are localized within one block–copolymer domain and can induce morphological transitions, such as from cylinder to lamellar structures.[7,20] Furthermore, a theoretical study on symmetric DBC–selective-NP mixtures confined between neutral walls using both self-consistent field theory (describing polymers) and density functional theory (describing NPs) shows that due to the entropic effects NPs are driven to the polymer–wall interfaces and favor parallel orientation of the lamellae with the NP selective block located near the walls.[16] This prediction is in agreement with our recent molecular dynamics simulation study where we observe parallel lamellae with NP selective blocks located near the neutral walls and the NPs are segregated in the polymer–wall interface forming a dense layer.[21] In the simulation, perpendicular lamellae are also observed, but only for nearly symmetric DBCs and at low values of NP concentration, whereas parallel morphologies are realized for symmetric as well as asymmetric DBCs and at relatively higher values of NP concentration.

[a]*Leibniz Institute of Polymer Research, Dresden, Germany. E-mail: shagolsem@ipfdd.de*
[b]*Institute of Theoretical Physics, TU Dresden, 01069 Dresden, Germany*

Several experimental and theoretical studies have addressed the commensurability and stability of parallel and perpendicular morphologies for pure DBC thin films – see ref. 22–28 – but to a lesser extent for DBC nanocomposite systems.[16,29,30] The problem of morphology selection (here mainly perpendicular *vs.* parallel) is of major interest for possible applications. Nanoparticles can influence on these morphologies and this might be an interesting and new possibility to control them. It has been observed in a recent experiment[29] that lamellae orientation can be changed using thermally stable gold NPs with tuned surface chemistry.

The freedom of the system to take up only a part of the NPs provided to the composite in order to minimize the free energy is most important for the parallel morphology. Here, controlled take-up can reduce the frustrations imposed by the film-thickness and might favor the parallel orientation. This effect becomes also important when the confining surfaces are selective with respect to one of the DBC phases. This is the problem we consider in the present work by using simple mean-field arguments. Here, with the mean-field method we maintain simplicity in the results without losing the complexity of the problem; also it forms the basis for a more complete description where various morphologies are taken into account.

Our aim here is to understand, considering a parallel morphology, the effect of NP concentration, film thickness and monomer–NP interaction in forming commensurable lamellae in the absence of enthalpic interactions between the polymer or NPs and walls (purely repulsive walls). An interesting scenario arises if particles can form a separated phase on top of the polymer layer. In this case uptake or release of nanoparticles can reduce frustration effects which originate from a mismatch of equilibrium lamellar period and the thickness of the layer. Furthermore, within the parallel morphology, we also study transition to wetting when the confining walls are selective. The rest of this work is organised as follows. In Section II, based on the strong segregation approximation,[31] we construct a simplified mean field free energy model for the DBC–selective-NP mixtures at a given composition confined in a slit of thickness L. We study the equilibrium properties of the nanocomposite considering both polymer non-selective walls in Section II, and selective walls in Section III. In both cases we consider a dense NP layer which can be formed in the polymer–wall interface; see Fig. 1. If the walls are selective with respect to the NP-selective block of the DBC we assume that for some value of the monomer–wall interaction the polymer can incorporate all the NPs and wet the surface. In Section III the transition to such "wetted" phase will be discussed and a corresponding phase diagram will be constructed.

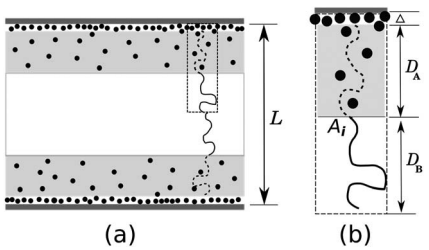

Fig. 1 (a) Schematic illustration of a horizontally oriented lamellar structure formed by a DBC–selective-NP mixture confined between two identical non-selective walls of separation L. NPs driven out of the polymer matrix form a dense layer of thickness Δ in the polymer–wall interface regions. (b) Magnification of the dotted region in (a): each chain with a fraction of NPs absorbed in it has a chain extension ($D_A + D_B$) and an A–B interface contact area A_i.

II. Mean-field model

In the strong stretching limit the pure phase of DBC forms a dry polymer brush.[31] Analogy between a polymer brush and DBC in the strong stretching limit has been exploited by Pryamitsyn and Ganesan to study density distribution of NPs and influence of NPs on the lamellar thickness and elastic constants of DBC.[32] It is important to note that unlike a surface grafted polymer brush the grafting density of a DBC-brush can vary depending on temperature and NP density. In our present study, we ignore effects of a non-homogeneous brush potential[33] and we consider a homogeneous distribution of particles inside the copolymer phases.

A. Non-selective walls

In Fig. 1(a), we sketch a single layer of horizontally oriented lamellae confined between two identical non-selective walls. Each chain has an interface contact area, A_i, and average heights, D_A and D_B, of the A and B blocks respectively; see Fig. 1(b). Since the NPs are selective with respect to the A-block the uptaken NPs are exclusively confined in the A-phase of the copolymer layer. A region of thickness Δ is formed at the polymer–wall interface by the NPs expelled from the polymer matrix as shown in Fig. 1(b). We consider this as a crystalline layer and set the free energy per NP to zero, *i.e.* consider this as the ground state of the NPs.

Let us assume that the preparation of the film consists of mixing a certain amount of NPs with a given amount of a DBC. The total number of NPs available per chain, n, remains an overall constant. The NP volume fraction, ϕ, is given by

$$\phi = \frac{n v_p}{N\sigma^3}, \tag{1}$$

where v_p and σ^3 are respectively the volumes of a NP and a Kuhn-monomer and we put $\sigma = 1$ for convenience, and N is the number of monomers in a chain. Suppose, N_A is the number of monomers in the A-block then the fraction of A is defined as $f = N_A/N$, and thus the number of monomers in the B-block is $N_B = N(1 - f)$. As shown in Fig. 1(b), if we denote the fraction of NPs absorbed in the A-phase of the copolymer by x then the condition of incompressibility is defined by the following set of equations

$$\begin{aligned} A_i \times D_A &= N(f + \phi x), \\ A_i \times D_B &= N(1 - f), \\ A_i \times d &= N\phi(1 - x). \end{aligned} \tag{2}$$

Here, we have defined an intensive quantity $d = \Delta/p$, the NP layer thickness per lamellar layer, where p is the number of lamellar layers. Furthermore, to accommodate p number of lamellar layers together with a NP layer of thickness Δ in between the walls separated by a distance L the condition of commensurability requires that

$$p(D + d) = L/2, \tag{3}$$

where $D = (D_A + D_B)$. The example in Fig. 1(a) corresponds to $p = 1$. From eqn (2) and (3), we get

$$A_i = \frac{2Np}{L}(1 + \phi), \tag{4}$$

$$d = \frac{L}{2p}\left(\frac{\phi - y}{1 + \phi}\right). \tag{5}$$

Here, we denote the uptake of nanoparticles in the A-phase of the copolymer film by y and it can be written as

$$y = \phi x: \quad 0 \le x \le 1, \tag{6}$$

but the expression for the optimal amount of NP uptake in terms of other fixed parameters of the system will be derived later in the section. The reduction in the thickness of the NP layer (per lamellar unit) due to the uptake of NPs in the polymer matrix is given by

$$\delta = d(y = 0) - d(y) = \frac{L}{2p}\left(\frac{y}{1 + \phi}\right). \tag{7}$$

Because of mass conservation δ is added to the particle selective A-block, thereby changing the overall chain extension. The contribution to the total free energy due to chain stretching and interface tension per chain, F_{DBC}, following the narrow interface approximation,[34] can be written as

$$F_{DBC} = \frac{3}{2N_A}\left(D_A{}^0 + \delta\right)^2 + \frac{3}{2N_B}D_B{}^2 + \chi^{1/2}A_i, \tag{8}$$

where χ is the effective Flory–Huggins interaction parameter where non-universal constants within the narrow interface approximation are taken into account. The first term in eqn (8) corresponds to the stretching of A-blocks, where $D_A{}^0 = f\left(\frac{L}{2p} - d(y = 0)\right) = \frac{L}{2p}\frac{f}{(1 + \phi)}$ is the thickness of the A-block for $y = 0$ and thus

$$D_A = \left(D_A{}^0 + \delta\right) = \frac{L}{2p}\left(\frac{f + y}{1 + \phi}\right); \tag{9}$$

The second term corresponds to the stretching of B-blocks with

$$D_B = \frac{L}{2p}\left(\frac{1 - f}{1 + \phi}\right). \tag{10}$$

In writing the free energy expressions we set the value of thermal energy, k_BT, to unity. We note that $D_A{}^0$ is obtained due to the geometrical restriction (confinement) and does not correspond to the equilibrium chain extension at zero NP uptake. The first and second terms together represent the stretching of the block-copolymer (F_{bc}).

The free energy contribution per chain due to the particles, F_{NP}, is given by the following expression,

$$F_{NP} = n_A\left[\ln(\eta) + \frac{4\eta - 3\eta^2}{(1 - \eta)^2}\right] - \varepsilon_p\eta N_A. \tag{11}$$

Here, $n_A = (yN_A/fv_p)$ is the number of NPs in the A-phase, η is the NP volume fraction within the A-phase given by $\eta = y/(f + y)$. The first term on the rhs of eqn (11) corresponds to the ideal translational entropy of a hard-sphere gas (F_{te}), while the second term is the non-ideal part approximated by the Carnahan–Starling equation (F_{cs}).[35] The third term represents the mean-field interaction of the polymer chain with the particles (F_{en}) at the given volume fraction η, and ε_p denotes the strength of monomer–NP attraction.

Adding eqn (8) and (11) we obtain the total free energy per chain,

$$F \simeq \frac{3}{2N_A}D_A{}^2 + \frac{3}{2N_B}D_B{}^2 + \chi^{1/2}A_i + n_A\left[\ln(\eta) + \frac{4\eta - 3\eta^2}{(1 - \eta)^2}\right] - \varepsilon_p\eta N_A, \tag{12}$$

where the expression for D_A and D_B are given by eqn (9) and (10) respectively.

Let us introduce a characteristic length scale ξ defined as

$$\xi = \left(\frac{\sqrt{\chi}}{3}\right)^{1/3}N^{2/3}\sigma \tag{13}$$

which corresponds to the equilibrium chain extension for a pure symmetric DBC melt in bulk obtained within the framework of our model.[11] In Fig. 2 we plot the total free energy F shown in eqn (12) at two different values of wall separation L as indicated in the figure. Here, the idea is to illustrate that the lamellae formed by the nanocomposites at a fixed value of L may be in a frustrated state and variation in the number of lamellar layers p can drive the system towards a higher/lower free energy state depending on the ratio of film thickness and equilibrium lamellar period. As shown in Fig. 2(a), for $L/2\xi = 1.0$, the system shows an increasing tendency of F for $p > 1$, whereas at $L/2\xi = 1.5$ – see Fig. 2(b) – it shows a decreasing tendency of F with increasing p. This suggests the existence of a preferred value of p at each value of L which minimizes the total free energy of the system.

For a given film thickness, L, the minimum of F with respect to the NP uptake $(\partial F/\partial y) = 0$ gives the equilibrium uptake of NPs as

$$\frac{3\xi^2(1 + y/f)}{N\rho^2} + \frac{N}{v_p}\left[\ln\left(\frac{y}{f + y}\right) + \frac{f}{f + y}\right] + t_{cs} - \frac{\varepsilon_p Nf}{(f + y)^2} = 0, \tag{14}$$

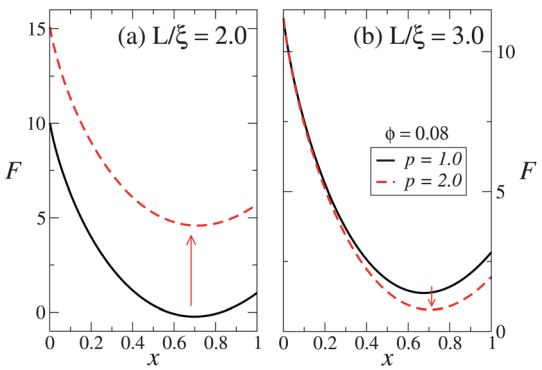

Fig. 2 Change in the total free energy per chain, $F(L, \phi)$, as a function of the absorbed fraction, x, of NPs for $\varepsilon_p = 0.001$, $\chi N = 100$, NP diameter $\sigma_p = 2\sigma$, and $f = 0.4$. Results are shown for $\phi = 0.08$, and for $p = 1$ and $p = 2$ at two different values of wall separation (a) $L/\xi = 2.0$ and (b) $L/\xi = 3.0$. Arrows indicate the direction of shift of the free energy curve upon changing the number of layers from 1 to 2.

where $t_{cs} \sim (8y/f + 3y^2/f^2)$ is the contribution from the Carnahan–Starling term and ρ is defined as

$$\rho = [1 - f + f(1 + y/f)^2]^{1/3}. \quad (15)$$

Eqn (14) in the limit $y \ll 1$ can be solved and it has the following form

$$y \sim f \exp[\nu_p(\varepsilon_p/f - (3\chi/N^2)^{1/3})], \quad (16)$$

and thus increasing N or ε_p increases the uptake y. An exact solution of eqn (14) at large values of y cannot be obtained as in the limit $y \ll 1$, and therefore we solve it numerically for large values of y to understand the equilibrium properties of the system. Now, at fixed L and y, the optimal number of lamellar layers p is obtained by setting $\left(\frac{\partial F}{\partial p}\right)_{L,y} = 0$ and it has the following expression

$$p = \frac{L}{2\xi}\frac{\rho}{(1+\phi)}. \quad (17)$$

Thus, at a fixed value of L and y, increasing ϕ would lead to a decrease in the optimal number of lamellar layers. A simultaneous solution of eqn (14) and (17) determines the equilibrium state of the polymer–nanocomposite at the given wall separation and overall nanoparticle fraction.

We take the copolymer nanocomposites in bulk as a reference state and the free energy contribution per chain in bulk, F_{bulk}, can be written as[11]

$$F_{bulk} \simeq \frac{3}{2N}D^2 + \chi^{1/2}\frac{N(1+y)}{D} + F_{NP}, \quad (18)$$

where D is the total extension of a DBC and F_{NP} is the NP contribution shown in eqn (11).

B. Numerical results

For the numerical calculations, we fix the values of χ (= 0.1) and N (= 1000) such that $\chi N = 100$ (strong segregation regime), and choose a diblock composition of $f = 0.4$. This choice of slightly asymmetric DBC is motivated by the simulation results[21] that for DBC–selective-NP mixtures confined by purely repulsive walls horizontally symmetric lamellae formed with the asymmetric DBC can be stable over a wide range of NP concentration values. Here, we use relatively small NPs *i.e.*, $\sigma_p = 2\sigma$, where σ and σ_p are respectively the monomer and NP diameters, and we vary the NP volume fraction ϕ in the range $0 \le \phi \le 0.8$. Within the mean-field treatment presented here the effects due to the inclusion of big NPs, *e.g.* chain conformations, cannot be captured accurately and thus we restrict to relatively small NPs. Numerical solutions of eqn (14) and (17) are obtained for the equilibrium NP uptake y, and the optimal number of lamellar layers p for a given film thickness L. In the following, we start with the discussion of fixed film thickness. For very thin films, *e.g.* $L/2\xi < 1$, the bulk equilibrium lamellar period cannot be realized and therefore we choose a film of thickness $L/\xi = 8.0$ so that the system can also realize the bulk values.

The equilibrium NP uptake, y, as a function of ϕ for a fixed wall separation of $L/\xi = 8.0$, is shown in Fig. 3. For a given value of monomer–NP interaction ε_p there is an optimal amount of NP uptake, y, given by eqn (14) and it is equal to the saturation threshold denoted by ϕ_s in the absorption isotherm shown in Fig. 3. As indicated by the plateau in the curve of y, for a given value of ε_p, there is no more uptake possible beyond the threshold value ϕ_s. However, in the region $\phi < \phi_s$ we see a linear increase with $y = \phi$ because of the value of ϕ being smaller than the value of optimal $y = \phi_s$ for the given ε_p and the NPs are completely absorbed by the copolymer film. The optimal amount of NP uptake increases with ε_p as shown in the inset of Fig. 3. Each point in the inset of Fig. 3 represents the average plateau height for the corresponding ε_p. A comparision of the various terms which contribute to the total free energy – see eqn (12) – is plotted as a function of ε_p as shown in Fig. 4. Here, for $\varepsilon_p > 0.2$, contributions from the Carnahan–Starling (F_{cs}) and the monomer–NP enthalpic interaction (F_{en}) terms dominate the other terms, and thus a higher NP uptake at large ε_p is limited mainly due to the large positive F_{cs} (packing) contribution.

In Fig. 5, we show the equilibrium free energy, $F(\phi)$, and the corresponding optimal number of lamellar layers, p, as a function of ϕ obtained at two different values of ε_p when $L/\xi = 8.0$.

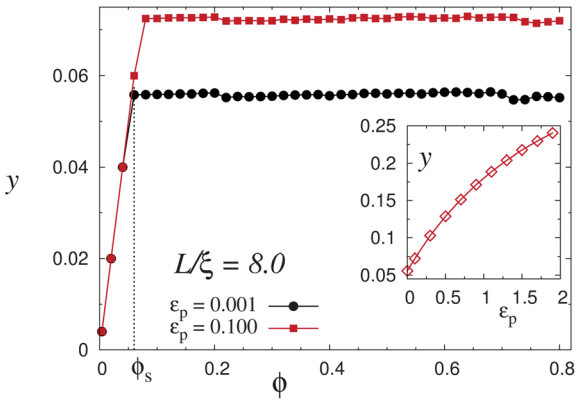

Fig. 3 Equilibrium uptake of NPs, y, as a function of ϕ for a given wall separation (L/ξ = 8.0) at ε_p = 0.001 and ε_p = 0.10. The saturation threshold, $\phi_s = 0.056$, is indicated for $\varepsilon_p = 0.001$. The quantity ϕ_s is equal to the optimal amount of NP uptake. Inset: the average plateau height as a function of ε_p.

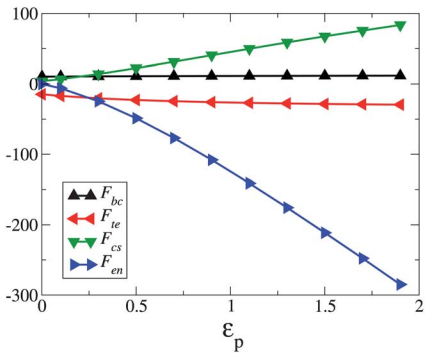

Fig. 4 Various terms which contribute to the total free energy (see eqn (12)) shown as a function of ε_p calculated at the optimal value of NP uptake shown in Fig. 3. Here, F_{bc}, F_{te}, F_{cs}, and F_{en} are respectively the chain stretching, translational entropy of NPs, Carnahan–Starling, and monomer–NP enthalpic interaction terms.

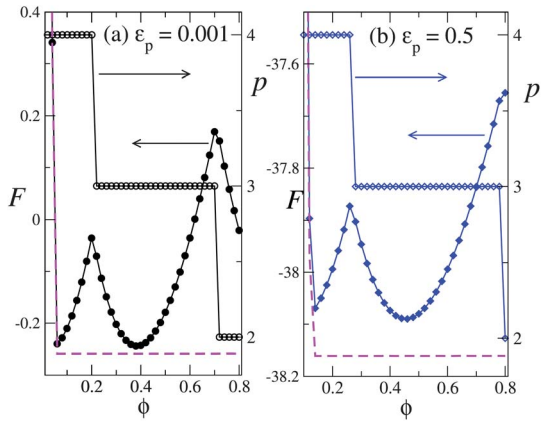

Fig. 5 Equilibrium free energy per chain, $F(\phi)$, and the corresponding optimal number of lamellar layers, p. The wall separation is fixed at $L/\xi = 8.0$. (a) $\varepsilon_p = 0.001$ and (b) $\varepsilon_p = 0.50$. Dashed lines represent the free energy in the bulk; see eqn (18).

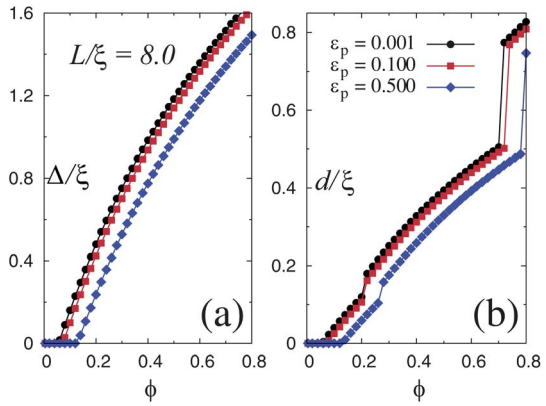

Fig. 6 Change in the (a) total thickness of the NP layer Δ, and (b) thickness of the NP layer per lamellar layer, d. Results are shown as a function of ϕ for three different values of ε_p indicated in the figure, and $L/\xi = 8.0$. Here, the NP layer thickness scales with ϕ as Δ or $d \sim \phi/(1+\phi)$.

Results are shown for (a) $\varepsilon_p = 0.001$ and (b) $\varepsilon_p = 0.50$. The free energy is lower for the higher value of A-monomer–NP attractive interaction ε_p; however, in both cases there is a decrease in the optimal value of p as we increase ϕ, and the change is associated with a cusp in the free energy curve. For higher values of ε_p the transition points are shifted to higher values of ϕ. The free energy displays a minimum for a given number of lamellar layers with respect to ϕ. It is interesting to note that, unlike the horizontal lamellae formed by a pure DBC, here the frustration present in the system at a given NP volume fraction can be reduced by changing the monomer–NP interaction strength alone. For example, the highly unfavorable points (cusp) in the free energy curve at $\phi \simeq 0.2$ and $\phi \simeq 0.65$ are shifted to the right upon increasing ε_p and thus reduce the frustration at that point; compare Fig. 5(a) and (b). This also illustrates the possible role of temperature T in reducing the frustration of nanocomposite films because the monomer–NP enthalpic interaction strength $\varepsilon_p \sim 1/T$.

The change in the thickness of the NP layer as a function of overall NP volume fraction, ϕ, for fixed L is shown in Fig. 6. The NP layer thickness vanishes for $\phi \leq \phi_s$ because below the threshold value ϕ_s all the NPs are absorbed in the polymer matrix; see also Fig. 3. Furthermore, the value of Δ is consistently lower for higher ε_p since the NP uptake y is higher for higher values of ε_p. Increase of total NP layer thickness Δ with ϕ is smooth, Fig. 6(a), and scales with ϕ as $\Delta \sim \phi/(1+\phi)$ according to eqn (5). However, the change of NP layer thickness per lamellar layer d has jumps, Fig. 6(b), due to the change in the optimal number of lamellar layers with increasing ϕ – see Fig. 5 – but the scaling with ϕ remains the same.

In Fig. 7 we display the change in equilibrium chain extension, D, with the variation of ϕ at a given value of wall separation $L/\xi = 8.0$. At low NP concentration ($\phi \leq \phi_s$) the chain extension is equal to that of pure DBC melts in the bulk, $D/\xi = 1.0$ (we have chosen a commensurable value of L), and D/ξ decreases with increasing ϕ above ϕ_s. Discontinuous relaxation of D/ξ to higher values is observed when ϕ is further increased. Thus, $D(\phi)$ at fixed L displays sawtooth-like behavior, and jumps in D are related to the transition of the number of lamellar layers. In accordance with the previous result, the value of ϕ when D is discontinuous increases for larger ε_p. In general, the chain extension oscillates about $D/\xi = 1.0$, and the maximum/minimum value depends on the film thickness and the number of lamellar layers.

Next, we consider the variation of the equilibrium free energy and the corresponding change in the optimal number of lamellar layers as we vary the film thickness. Here, we fix ϕ and determine the lowest free energy state by varying the NP uptake, y, and the number of lamellar layers, p, for a given L, and then we vary L in the range $1 \leq L/\xi \leq 10$. In Fig. 8, we display the optimal free energy, $F(L)$, and corresponding optimal number of lamellar layers, p, obtained at different values of NP concentration, ϕ, indicated in the figure while keeping $\varepsilon_p = 0.001$. As we can see in Fig. 8(a), for larger ϕ the free energy curve as a whole is shifted to the right *i.e.*, minima positions moved to higher values of L/ξ. This behavior can be understood if we recall the fact that increasing ϕ above the saturation threshold ϕ_s creates a NP layer whose thickness increases with increasing ϕ – see Fig. 6(a) – and thus a larger value of L corresponds to the optimal free energy at larger ϕ when ε_p is fixed. In order to rationalize this behavior we

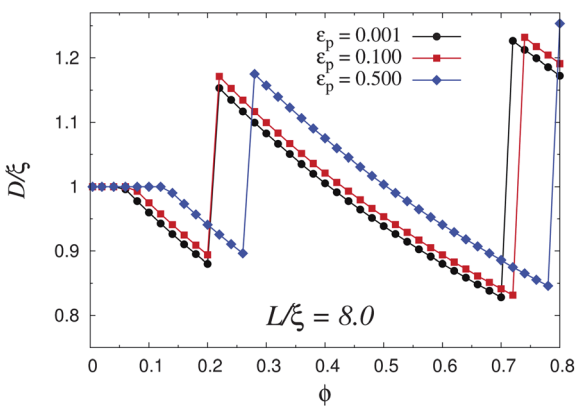

Fig. 7 Chain extension, D, as a function of ϕ calculated at a film thickness $L/\xi = 8.0$. Results are shown for $\varepsilon_p = 0.001$, 0.1 and 0.5. Jumps in the value of D correspond to the jumps of p in Fig. 5.

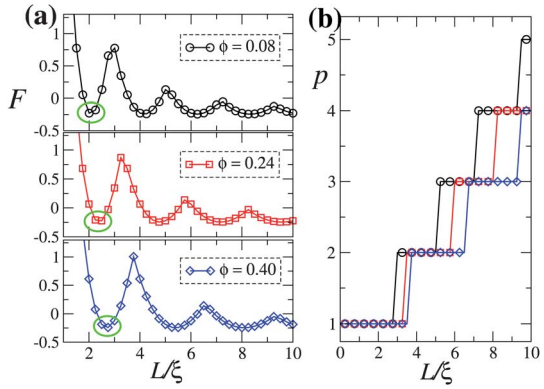

Fig. 8 (a) Equilibrium free energy and (b) corresponding optimal number of lamellar layers as a function of wall separation, L/ξ, at ϕ = 0.08, 0.24 and 0.40 while keeping $\varepsilon_p = 0.001$. The first minimum in the free energy curves is encircled to highlight the shift along the X-axis with increasing ϕ; see (a).

consider the rescaled film thickness $\tilde{L} \equiv L/L_1$, where L_1 is the film thickness at which $F(L)$ has the first minimum; see Fig. 8(a). If we now plot F as a function of rescaled film thickness we see that the free energy curves for different ϕ fall on top of each other, and thus $F(\tilde{L})$ no longer has ϕ dependence; see Fig. 9. The positions of the minima correspond to the optimal film thickness for $p = 1, 2, 3$ and so on. We observed similar behavior for other values of ε_p. The rescaled form of the free energy curve displayed in Fig. 9 can be obtained directly from eqn (12) as shown below.

The equilibrium film thickness, $\bar{L}$, at fixed y and p for a given ϕ is obtained by setting $\left(\frac{\partial F}{\partial L}\right)_{y,p} = 0$, and it has the following expression

$$\bar{L} = 2p(1 + \phi)\xi\rho^{-1}. \tag{19}$$

Thus,

$$L_1 = \bar{L}_{p=1} = 2(1 + \phi)\xi\rho^{-1}, \tag{20}$$

and using this expression of L_1 in eqn (12), we get

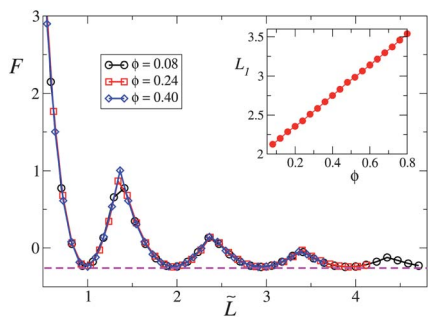

Fig. 9 Equilibrium free energy per chain, F, shown in Fig. 8(a), plotted as a function of rescaled film thickness $\tilde{L} = L/L_1$; see text for the definition of L_1. The dashed line represents the free energy in the bulk; see eqn (18). Inset: change of L_1 as a function of ϕ.

$$F \simeq \frac{3}{2N}\left(\frac{\tilde{L}\xi}{p}\right)^2 \rho^{-1} + \chi^{1/2} N\rho\left(\frac{p}{\tilde{L}\xi}\right) + n_A\left[\ln(\eta) + \frac{4\eta - 3\eta^2}{(1-\eta)^2}\right] - \varepsilon_p \eta N_A. \tag{21}$$

Here, by introducing the rescaling film thickness $\tilde{L} = L/L_1$, the free energy F no longer depends on ϕ as in Fig. 9. The dependence of ϕ enters only in L_1; see eqn (20).

In Fig. 10 we display the value of equilibrium chain extension, D, as a function of rescaled film thickness $\tilde{L}$ when $\varepsilon_p = 0.001$. As we can see, the value of D/ξ oscillates around 1 and amplitude decreases with increasing film thickness. Since the NP uptake at $\varepsilon_p = 0.001$ is very low – see Fig. 3 – it is expected that D/ξ will finally converge to 1 at very large values of L. The behavior of chain extension shown here for the nanocomposites is almost the same as that obtained experimentally by T. P. Russell and coworkers for a pure symmetric DBC in confinement.[36]

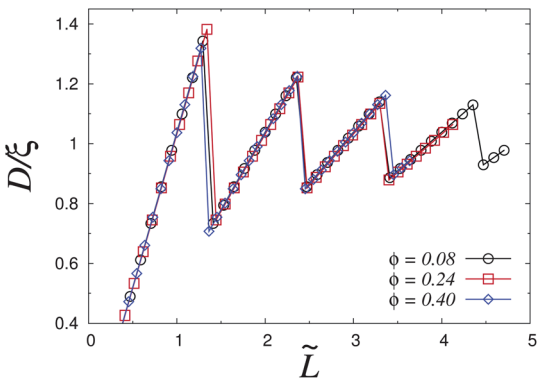

Fig. 10 Equilibrium chain extension, D, as a function of rescaled film thickness, $\tilde{L}$, calculated at different values of ϕ while keeping $\varepsilon_p = 0.001$.

III. Selective walls and phase diagram

A. Mean field model

For non-selective walls, above the saturation threshold ϕ_s a NP layer of thickness $\Delta > 0$ is formed and separates the wall from the DBC. If the walls are attractive with respect to A-monomers then for some values of monomer–wall interaction the A-phase could wet the surface by uptaking all the NPs.

To study the case of selective walls, we add a monomer–wall interaction term to the free energy given by eqn (12). Contribution to the total free energy due to the A-monomer–wall interaction is denoted by F_w, and it is approximated by the product of an effective monomer density near walls c_A and the monomer–wall interaction strength per chain γA_i:

$$F_w = -\gamma A_i \times c_A, \tag{22}$$

where γ is the interaction strength per unit area. Assuming a homogeneous NP distribution inside the A-phase, we define the effective monomer density near walls as

$$c_A = 1 - \alpha\left(\frac{\phi}{f + \phi}\right), \tag{23}$$

where $\alpha = (a_d/v_p)\sigma$ with a_d as the area of the monomer depletion region on the walls due to a NP close to the wall. According to

Fig. 11 we obtain $a_d = \pi\sigma\sigma_p$. The second term on the rhs of eqn (23) represents the overall reduction of the monomer–wall contact area due to NPs in the vicinity of walls. The total free energy for the "wetted" F_1 is

$$F_1 = F_{y=\phi} + F_w. \quad (24)$$

If a transition to the wetted phase from the non-wetted phase is possible then the following condition must be fulfilled

$$\Delta F \leq 0, \quad (25)$$

where $\Delta F = F_1 - F$ is the free energy difference between the wetted (eqn (24)) and the non-wetted (eqn (12)) phases for a given ϕ and L. Eqn (25) at equality gives the critical value γ^*.

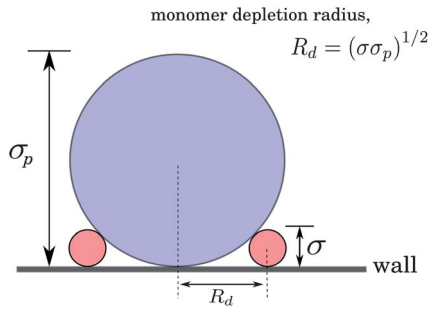

Fig. 11 Schematic illustration of the monomer depletion region due to a nano-particle close to the wall. On the wall, a region of radius R_d from the center of a NP is not available to monomers. The depletion radius, depending on the particle size, varies as $R_d = \sigma_p/\sqrt{m}$, where $m = \sigma_p/\sigma$, and thus the area of the depletion region $a_d = \pi\sigma_p^2/m$.

B. Numerical results and phase diagram

In this section, using numerical calculations, we will discuss the transition between the "wetted" and the "non-wetted" phases as a function of NP volume fraction ϕ for a film of thickness $L/\xi = 8.0$. For the numerical calculations, we first optimize the free energy for the "wetted" case F_1 by varying p for a fixed value of γ and L and at $y = \phi$ for a given ϕ. Next, we calculate the free energy F according to eqn (12) for the equilibrium values of p and y. Using eqn (25) we calculate γ^* for which the equality is exactly fulfilled.

In Fig. 12(a), we display the phase diagram in the $\phi - \gamma$ plane showing "wetted" and "non-wetted" phases. Since, for ϕ below the saturation threshold, ϕ_s, there is a complete uptake of nanoparticles in the A-phase – see Fig. 3 – the free energy difference between the two phases $\Delta F = 0$. Thus, the critical value of interaction strength $\gamma^* = 0$ for $\phi < \phi_s$. However, when $\phi > \phi_s$ we have $\Delta F \neq 0$ and thus obtain a non-zero γ^* and the value of γ^* increases rapidly on further increase of ϕ. As we can see in Fig. 12(a), the value of γ^* decreases upon increasing ε_p at a given value of ϕ and this is due to the higher NP uptake at large values of ε_p. This shift of the coexistence line shows the broadening of the wetted phase. Also when crossing the coexistence line in the region $\gamma^* \neq 0$, there is jump in the number of optimal lamellar layers p – see Fig. 12(b) – and a corresponding jump in chain

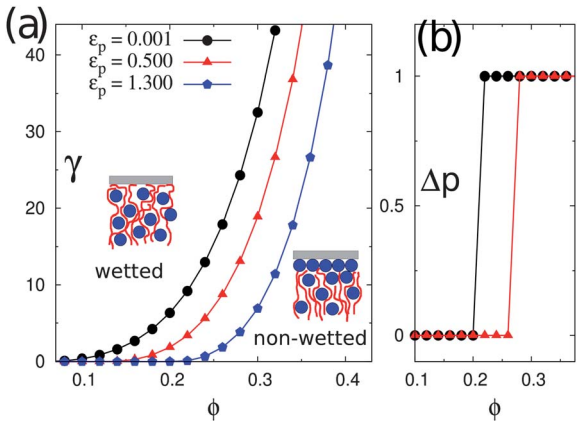

Fig. 12 (a) Phase diagram: lines separating "wetted" and "non-wetted" regions – shown for three different values of ε_p for $L/\xi = 8.0$. Above the line is the "wetted" phase while that below is the "non-wetted" phase. The coexistence line is shifted to the right for higher ε_p indicating the broadening of the wetted region. (b) Difference in the optimal number of lamellar layers Δp between the two phases.

extension D in going from the "non-wetted" to "wetted" phase. This indicates a discontinuous (first order) transition between the two different phases.

IV. Conclusion

We have presented a simplified mean field model, based on the strong segregation theory, for a mixture of A–B diblock copolymers and A-block selective NPs confined between two identical walls in slit geometry. A horizontally oriented lamellar structure of the nanocomposite is considered. Here, nanoparticles can be segregated at the walls in order to reduce the frustration of incommensurabilty and lower the free energy of the parallel morphology.

The equilibrium state of our system is determined by simultaneously varying the NP uptake in the A-phase and the number of copolymer layers formed between the walls. Both non-selective and A-block selective wall types are considered. With the non-selective walls, in particular, we have discussed the NP uptake behavior and effects of particle concentration and film thickness in forming commensurable lamellae. Also the transition to a wetted phase when the confining walls are selective is considered.

In non-selective walls case, at very low NP concentration, a complete uptake of NPs is driven by enthalpic interactions with the A-phase (under-saturated regime). At higher concentrations a dense layer of NPs at the polymer–wall interface is formed and the uptake of particles is limited mainly by concentration effects which are taken into account by the Carnahan–Starling term in the free energy (saturated regime). If the concentration of nanoparticles is increased further keeping a fixed distance between the walls the optimal number of lamellar layers decreases jump-like. The change in the optimal number of layers results in a discontinuous transition of the chain's extension and is associated with a cusp in the free energy. An interesting result that we observed here is that it is possible to reduce the frustration in a film of fixed thickness by properly tuning the monomer–NP interaction strength ε_p; see Fig. 5.

An attractive (selective) interaction between A-monomers and walls leads to a discontinuous transition between "non-wetted" and "wetted" phases. For the latter a complete uptake of particles is more favorable due to the contact energy gained by the A-phase. Based on our free energy arguments a phase diagram in the plane of nanoparticle-fraction and monomer–wall interaction has been constructed. In general, we observe broadening of the "wetted" region upon increasing the nanoparticle–monomer interaction. The transition between the two phases is discontinuous related to a jump in the optimal number of lamellar layers.

An interesting question is the selection of lamellar reorientations and possible morphological transitions induced by the NPs. Here, one has to compare several scenarios of where the segregated NPs are placed. If we neglect the problem of location of segregated NPs within the film the free energy of the perpendicular orientation corresponds to that of the bulk state with the optimal take-up of NPs. In our calculations this leads generally to lower free energies – see Fig. 5 and 9 – and thus to a preference of perpendicular orientation for non-selective walls. This result, however, contradicts recent SCFT calculations[16] and direct MD simulations.[21] Thus, a more detailed approach to the perpendicular morphology of the nanocomposite including the problem of the free energy effort of forming a segregated NP-phase is necessary.

Acknowledgements

Financial support from DFG (under grant SO-277/3-1) is gratefully acknowledged. The work is also funded by the European Union (ERDF) and the Free State of Saxony via TP A2 ("MolDiagnostik") of the Cluster of Excellence "European Center for Emerging Materials and Processes Dresden" (ECEMP). L. S. Shagolsem acknowledges support from the ECEMP - International Graduate School.

References

1 M. Templin, *et al.*, *Science*, 1997, **278**, 1795.
2 D. Zhao, *et al.*, *Science*, 1998, **279**, 548.
3 S. Stupp and P. V. Braun, *Science*, 1997, **277**, 1242.
4 Y. Zhao, *et al.*, *Nat. Mater.*, 2009, **8**, 927.
5 I. W. Hamley, *The Physics of Block Copolymers*, Oxford University Press, 1998.
6 J. J. Chiu, B. J. Kim, E. J. Kramer and D. J. Pine, *J. Am. Chem. Soc.*, 2005, **127**, 5036–5037.
7 J. Huh, V. V. Ginzburg and A. C. Balazs, *Macromolecules*, 2000, **33**, 8085.
8 V. Lauter-Pasyuk, H. J. Lauter, D. Ausserr, Y. Gallot, V. Cabuil, E. I. Kornilov and B. Hamdoun, *Physica B*, 1998, **1092**, 241–243; V. Lauter-Pasyuk, H. J. Lauter, D. Ausserr, Y. Gallot, V. Cabuil, E. I. Kornilov and B. Hamdoun, *Physica B*, 1998, **248**, 243; V. Lauter-Pasyuk, H. J. Lauter, G. P. Gordeev, P. Müller-Buschbaum, B. P. Toperverg, M. Jernenkov and W. Petry, *Langmuir*, 2003, **19**, 7783.
9 B. J. Kim, J. J. Chiu, G.-R. Yi, D. J. Pine and E. J. Kramer, *Adv. Mater.*, 2005, **17**, 2618–2622.
10 B. J. Kim, G. H. Fredrickson, C. J. Hawker and E. J. Kramer, *Langmuir*, 2007, **23**, 7804–7809.
11 L. S. Shagolsem and J.-U. Sommer, *Macromol. Theory Simul.*, 2011, **20**, 329–339.
12 A. C. Balazs, T. Emrick and T. P. Russell, *Science*, 2006, **314**, 1107.
13 S. Gupta, Q. Zhang, T. Emrick, A. C. Balazs and T. P. Russell, *Nat. Mater.*, 2006, **5**, 229.
14 R. S. Krishnan, M. E. Mackay, P. M. Duxbury, C. J. Hawker, S. Asokan, M. S. Wong, R. Goyette and P. Thiyagarajan, *J. Phys.: Condens. Matter*, 2007, **19**, 356003.
15 J. Y. Lee, Z. Shou and A. C. Balazs, *Phys. Rev. Lett.*, 2003, **91**, 136103.
16 J. Y. Lee, Z. Shou and A. C. Balazs, *Macromolecules*, 2003, **36**, 7730.
17 E. S. McGarrity, A. L. Frischknecht, L. J. D. Frink and M. E. Mackay, *Phys. Rev. Lett.*, 2007, **99**, 238302.
18 E. S. McGarrity, A. L. Frischknecht and M. E. Mackay, *J. Chem. Phys.*, 2008, **128**, 154904.
19 R. S. Krishnan, M. E. Mackay, P. M. Duxbury, A. Pastor, C. J. Hawker, B. van Horn, S. Asokan and M. S. Wong, *Nano Lett.*, 2007, **7**, 484.
20 S. G. Jang, A. Khan, C. J. Hawker and E. J. Kramer, *Macromolecules*, 2012, **45**, 1553.
21 L. S. Shagolsem and J.-U. Sommer, manuscript in preparation.
22 M. S. Turner, *Phys. Rev. Lett.*, 1992, **69**, 1788.
23 D. G. Walton, G. J. Kellogg, A. M. Mayes, P. Lambooy and T. P. Russell, *Macromolecules*, 1994, **27**, 6225.
24 A. L. Frischknecht, J. G. Curro and L. J. D. Frink, *J. Chem. Phys.*, 2002, **117**, 10398.
25 T. Geisinger, M. Müller and K. Binder, *J. Chem. Phys.*, 1999, **111**, 5241.
26 P. Mansky, Y. Liu, E. Huang, T. P. Russell and C. Hawker, *Science*, 1997, **275**, 1458.
27 P. Mansky, T. P. Russel, C. J. Hawker, M. Pitsikalis and J. Mays, *Macromolecules*, 1997, **30**, 6810.
28 J.-U. Sommer, A. Hoffmann and A. Blumen, *J. Chem. Phys.*, 1999, **111**, 3728.
29 M. Yoo, S. Kim, S. G. Jang, S.-H. Choi, H. Yang, E. J. Kramer, W. B. Lee, B. J. Kim and J. Bang, *Macromolecules*, 2011, **44**, 9356.
30 J. G. Son, H. Kang, K.-Y. Kim, J.-S. Lee, P. F. Nealey and K. Char, *Macromolecules*, 2012, **45**, 150.
31 A. N. Semenov, *Sov. Phys. - JETP*, 1985, **61**(4), 733.
32 V. Pryamitsyn and V. Ganesan, *Macromolecules*, 2006, **39**, 8499.
33 A. Halperin and M. Kröger, *Langmuir*, 2009, **25**(19), 11621.
34 E. Helfand and Z. R. Wasserman, *Macromolecules*, 1976, **9**, 879.
35 N. F. Carnahan and K. E. Starling, *J. Chem. Phys.*, 1969, **51**, 635.
36 T. P. Russell, *et al.*, *Physica B*, 1995, **213/214**, 22.